ChemPubSoc Europe
DOI: 10.1002/chem.201504955
CHEMISTRY A European Journal
Full Paper

Medicinal Chemistry |Hot Paper|

Synthesis and Biological Evaluation of Novobiocin Core Analogues as Hsp90 Inhibitors

Katherine M. Byrd,[a] Chitra Subramanian,[b] Jacqueline Sanchez,[b] Hashim F. Motiwala,[b] Weiya Liu,[c] Mark S. Cohen,[b] Jeffrey Holzbeierlein,[c] and Brian S. J. Blagg*[a]

Abstract: Development of heat shock protein 90 (Hsp90) C-terminal inhibitors has emerged as an exciting strategy for the treatment of cancer. Previous efforts have focused on modifications to the natural products novobiocin and coumermycin. Moreover, variations in both the sugar and amide moieties have been extensively studied, whereas replacements for the coumarin core have received less attention. Herein, 24 cores were synthesized with varying distances and angles between the sugar and amide moieties. Compounds that exhibited good anti-proliferative activity against multiple cancer cell lines and Hsp90 inhibitory activity, were those that placed the sugar and amide moieties between 7.7 and 12.1 Å apart along with angles of 180°.

Introduction

Heat shock protein 90 (Hsp90) is a molecular chaperone that is responsible for folding nascent polypeptides into their biologically active conformation. More than 200 client proteins depend upon Hsp90 for their maturation/activation, and many are essential to cancer cell survival and proliferation.[1–4] Unlike drugs that target these individual client proteins, inhibition of Hsp90 results in the degradation of more than 30 anticancer targets simultaneously. Furthermore, Hsp90 is overexpressed and can be selectively targeted in cancer, thus its inhibition can diminish potential side effects.[5–7]

Seventeen Hsp90 inhibitors have entered clinical trials for the treatment of cancer. All of these inhibitors bind the N-terminal ATP binding site.[8–10] The major problem associated with these inhibitors is induction of the heat shock response (pro-survival) at the same concentration that leads to protein degradation. Due to increased Hsp90 levels observed upon administration of N-terminal inhibitors, the scheduling and dosing of patients is often difficult.[11] Presently, no Hsp90 inhibitor is FDA-approved for the treatment for cancer.

In contrast to N-terminal inhibitors, C-terminal inhibitors can be prepared that do not induce the pro-survival heat shock response that is responsible for these dosing difficulties.[12] In fact, Hsp90 C-terminal inhibitors have proven to exhibit distinct properties when compared to N-terminal inhibitors.[13,14] Therefore, the development of Hsp90 C-terminal inhibitors could provide a clinically useful alternative for the treatment of cancer.[15–19]

Studies have shown that natural product C-terminal inhibitors,[20–24] such as novobiocin and coumermycin A1, do not induce the heat shock response. Unfortunately, these compounds manifest IC_{50} values of 700 and 70 μм, respectively.[25,26] Although no crystal structure of the Hsp90 C terminus bound to inhibitors exists, homology models have been developed to aid the design of new inhibitors.[27–29] Using these models, structure–activity-relationship (SAR) studies on novobiocin and coumermycin have led to compounds that manifest activity in the mid to low nanomolar range against a variety of cancers,[30] which supports the potential use of these compounds as anticancer therapeutics.

To date, SAR studies on novobiocin have primarily focused on finding replacements for the noviose sugar and the prenylated aryl side chain (Figure 1). In fact, more potent Hsp90 inhibitors can be accessed by replacement of the noviose sugar with *N*-methylpiperidine (**2**) or by substitution of the prenylated aryl side chain with a biaryl side chain (**3**).[31] Both of these modifications not only lead to more efficacious analogues, but also a simplified synthesis, as the noviose sugar requires more than 10 synthetic transformations. In addition to the coumarin core, biaryl cores (**4** and **5**) have been discovered that manifest superior anticancer activity.[32] Since compounds containing a biaryl core exhibit improved inhibitory activity over the coumarin-based compounds, it suggests that some flexibility within the C-terminal binding pocket may exist. Additionally, orientation of the *N*-methylpiperidine and the biaryl side chain may also be important for the increased efficacy. In fact, compounds prepared to date project the sugar and amide side chains linearly at approximately 180°. Therefore, the focus of

[a] K. M. Byrd, Prof. B. S. J. Blagg
Department of Medicinal Chemistry, The University of Kansas
Wescoe Hall Drive, Malott 4070, Lawrence, KS 66045-7563 (USA)
E-mail: bblagg@ku.edu

[b] C. Subramanian, J. Sanchez, H. F. Motiwala, Prof. M. S. Cohen
Department of Surgery, University of Michigan, Ann Arbor, MI 48109 (USA)

[c] W. Liu, Prof. J. Holzbeierlein
Department of Urology, The University of Kansas Medical Center
3901 Rainbow Boulevard,Stop 3016, Kansas City, Kansas 66160 (USA)

Supporting information for this article is available on the WWW under http://dx.doi.org/10.1002/chem.201504955.

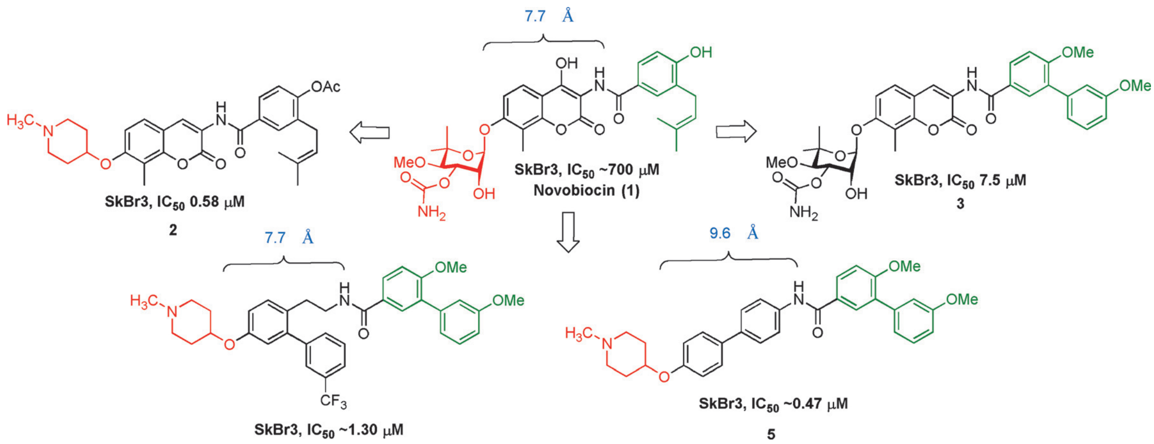

Figure 1. Novobiocin and analogues previously evaluated.

this study was to determine the optimal distance and angle between the *N*-methylpiperidine and the biaryl side chain.

Results and Discussion

Design and synthesis of novel scaffolds

In order to determine the optimal distance and angle between the *N*-methylpiperidine and the biaryl side chain, cores were designed to place these groups between 6.2 and 14.3 Å apart as presented in Table 1.

From a design perspective, initial efforts were focused on modification of the bicyclic core represented by the coumarin ring in novobiocin. First, the biaryl side chain was placed at the 1-position of both the tetrahydronaphthalene and naphthalene cores (**6** and **7**). Second, the biaryl side chain was placed at the 2-position of the tetrahydronaphthalene core. Compounds **6**–**8** would provide insight into both the position and planarity of the biaryl side chain on the bicyclic ring system.

Next, a series of compounds with a three-ring core was designed. The first set of compounds contained a phenylnaphthalene core, wherein the biaryl side chain or the *N*-methylpiperidine was placed at all three positions on the benzene ring (Figure 2). A variety of distances and angles could be quickly accessed with this scaffold, as advanced intermediates could be used for the preparation of additional compounds.

The second set of compounds investigated were the 1-phenyl-di(tetra)hydronaphthalene analogues (**15**–**18**). Initially, the 1-phenyl-dihydronaphthalene scaffold was designed to compare placement of the phenyl ring on the 1- versus 2-position of the naphthalene ring. Later, 1-phenyl-tetrahydronaphthalene analogues could also be accessed by use of an intermediate. The 1-phenyl-tetrahydronaphthalene scaffold would provide data on planarity of the three-ring system and its effect on anti-proliferative activity. The third set of compounds contained two fused three-ring cores (**19** and **20**). Unlike the previous sets of compounds, where one of the rings was able to rotate freely, the fused ring system provides ridged counterparts for investigation. A comparison of anti-proliferative activities between these compounds would help establish the role played by the core.

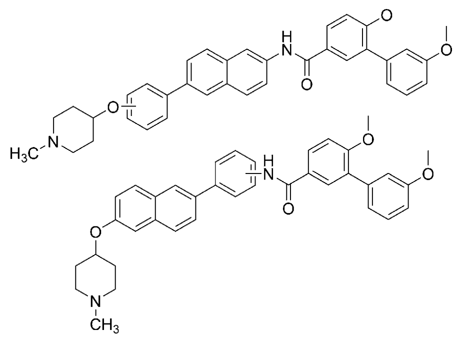

Figure 2. Analogues with phenyl-naphthalene core.

Compounds **21** and **22** contain 4-ring analogues that were designed for this investigation. Additionally, compound **23** represents a derivative of **5**, where an alkyne was placed between the phenyl rings to increase distance between the *N*-methylpiperidine and the biaryl side chain by two carbons, while maintaining linearity. The alkyne in **23** could be reduced to both the alkene (**24** and **25**) and alkane (**26**) to provide insights into the flexibility and geometry of the two-carbon linker. Finally, an additional series of alkyne-containing compounds was envisioned (**27**–**29**) that extend from an aromatic core.

Various angles between the *N*-methylpiperidine and the biaryl side chain were accessed by placement of these groups at different positions within the same core structure. Compounds **9**, **11** and **13** are representative examples wherein this strategy was utilized. Alternatively, different angles were observed when the biaryl side chain was placed out of plane with regards to the core (Figure 3).

Synthesis of select analogues

Scheme 1 illustrates the synthetic protocol used to prepare 1-amido and 2-amido analogues. Amines **30 a/b**, which were synthesized from the corresponding 6-methoxy-tetralones (see the Supporting Information), were subjected to EDCI coupling

Table 1. List of cores with varying distance and angles.

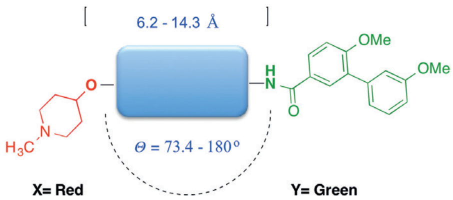

Cmpd	Structure	Dist. [Å][a,b]	Angle [°][b]
6	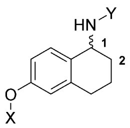	6.2	73.4
7	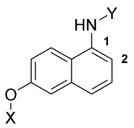	6.3	120
8	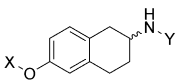	7.8	160.9
9	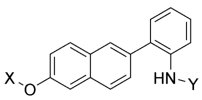	7.7	115
10	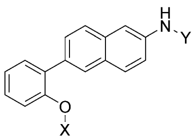	7.9	115
11	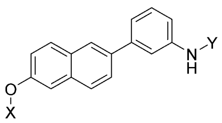	10.4	139.3
12	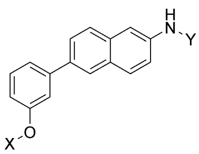	10.5	141.6
13	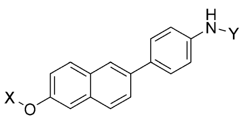	11.8	168.9
14	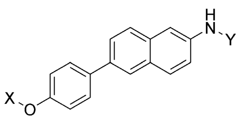	11.8	172.1
15	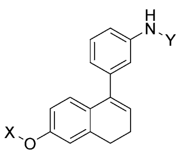	7.8	79.4
16	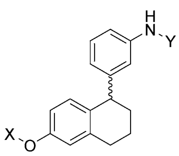	9.1	118.8

Table 1. (Continued)

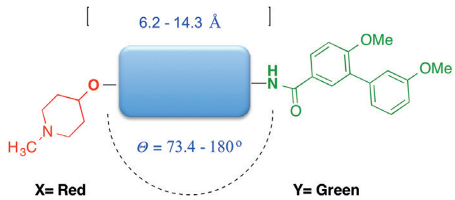

Cmpd	Structure	Dist. [Å][a,b]	Angle [°][b]
17	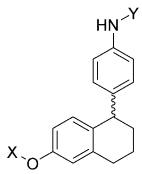	9.2	108.3
18	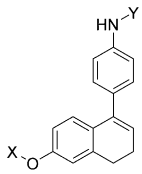	9.8	104.3
19	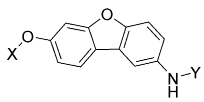	9.1	124.6
20	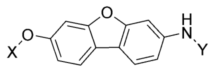	9.4	154.5
21	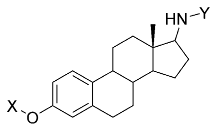	9.2	168.3
22	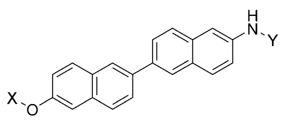	14.1	180
23	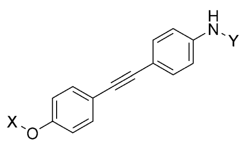	12.1	180
24	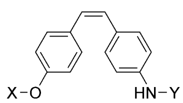	9.1	120
25	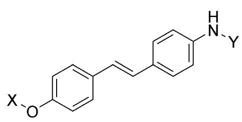	11.8	170.7
26	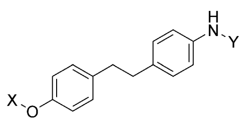	11.9	166.6
27	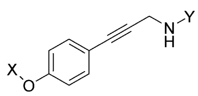	8.7	163

Table 1. (Continued)

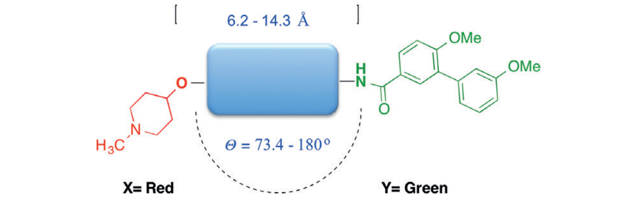

Cmpd	Structure	Dist. [Å][a,b]	Angle [°][b]
28	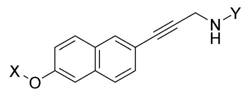	10.9	172.2
29	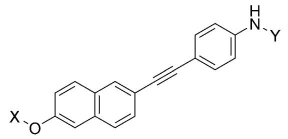	14.3	160.5

[a] Distance measured between the oxygen bound to *N*-methylpiperidine and amide nitrogen of the biaryl side chain. [b] Both distance and angles were measured in PyMOL after the 3D structures had been minimized through molecular dynamic simulations.

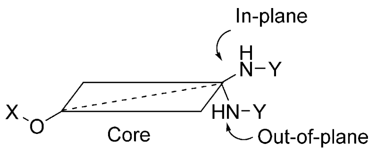

Figure 3. Graphic representation of the biaryl side chain that rests either in or out-of-plane.

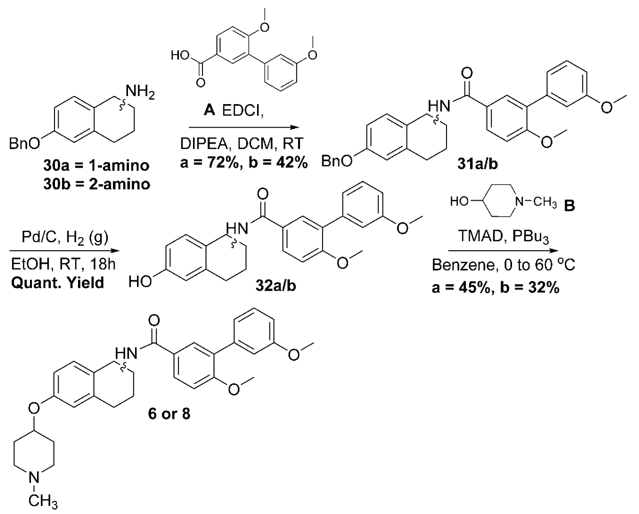

Scheme 1. Synthesis of 1 and 2-amido novobiocin analogues.

with carboxylic acid **A**. After removal of the benzyl group by hydrogenolysis, phenol **32 a/b** was coupled with *N*-methyl-4-piperidinol (**B**) through Mitsunobu etherification.[33]

A representative synthesis of the phenylnaphthalene analogues is shown in Scheme 2. Synthesis began by the coupling of commercially available 2-amino-6-bromonaphthalene (**33**) with **C** to form amide **34** in good yield. Amide **34** was the common intermediate used to prepare analogues wherein the *N*-methylpiperidine was placed at all three positions on the phenyl substituent. A Suzuki coupling between amide **34** and boronic acids **35 a–c** produced the phenylnaphthalenes, **36 a–c**, in moderate yield. Finally phenols **36 a–c** were coupled with **B** through a Mitsunobu reaction to generate the final products (**10**, **12**, **14**) in 53–60 % yield.

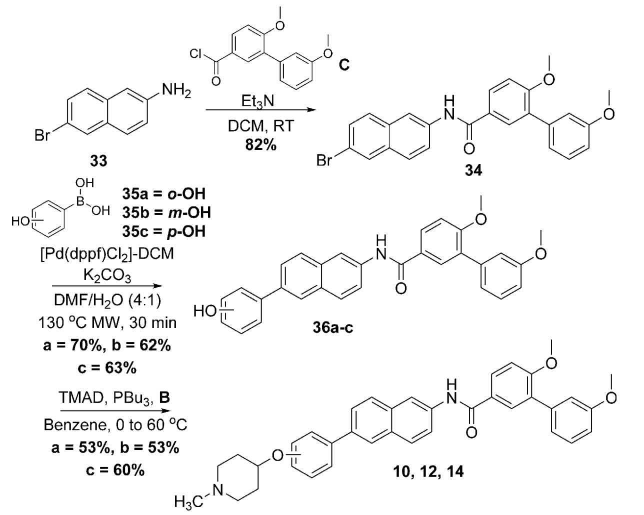

Scheme 2. Synthesis of 2-phenyl-naphthalene analogue.

Synthesis of 1-phenyl-di(tetra)hydronaphthalene analogues commenced by a Suzuki coupling between commercially available boronic acids, **38 a/b**, and vinyl triflate **37**[34] to yield the corresponding nitro aromatics, **39 a/b** (Scheme 3). Following demethylation of **39 a/b**, *N*-methyl-4-piperidinol was coupled with phenols **40 a/b** under Mitsunobu conditions. At this point, the synthesis diverged and the nitro group in **41 a/b** selectively reduced to the corresponding aniline using iron-catalyzed conditions (**42 a/b**); or both the nitro group and the alkene were reduced via a palladium-catalyzed hydrogenation (**43 a/b**). The resulting anilines were then coupled with acid chloride **C** to form amides **15/18** or **16/17**, respectively.

Preparation of the dibenzo[*b*,*d*]furan cores is shown in Scheme 4.[35] Synthesis of the dibenzofuran-containing analogues began by a Suzuki coupling between boronic acid **44** and aryl bromides **45 a/b** to yield **46 a/b** in moderate yield. Pyridine-HCl was used to cleave the methyl ethers of **46 a/b** and provide resorcinols **47 a/b**. An intramolecular nucleophilic substitution of the resorcinol moiety (**47 a/b**) generated dibenzofuranols **48 a/b** in good yields. *N*-Methyl-4-piperidinol was added to **48 a/b** through a Mitsunobu reaction, which produced **49 a/b**. Following reduction of the nitro group present in **49 a/b**, the resulting aniline was coupled with acid chloride **C** to furnish **19** and **20**.

The synthesis of an alkyne-containing compound is outlined in Scheme 5. Commercially available 4-ethynylanisole (**51**) was coupled with 1-bromo-4-nitrobezene (**52**) under Sonogashira

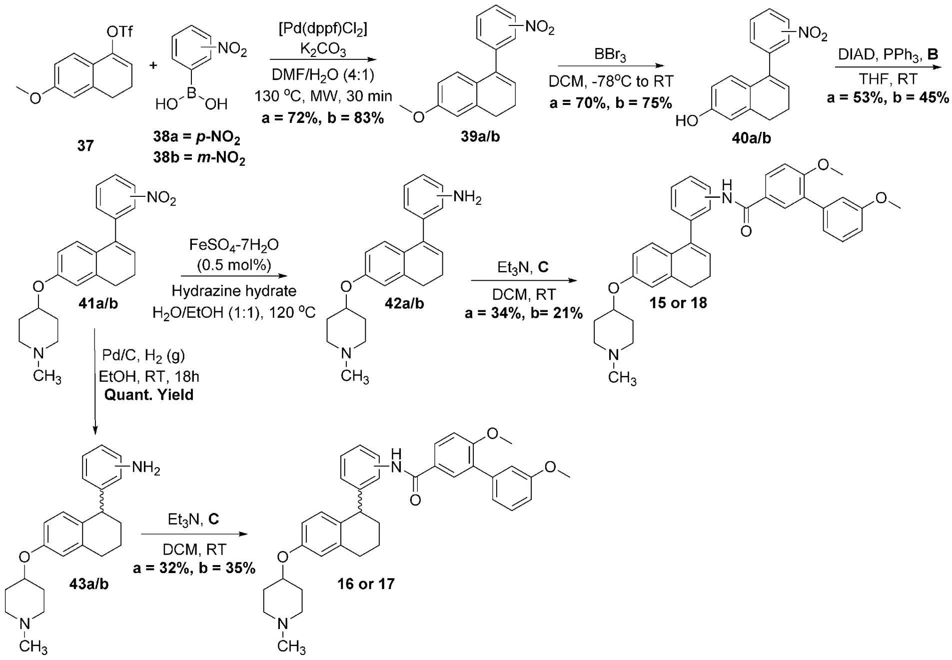

Scheme 3. Synthesis of 1-phenyl-di(tetra)hydronaphthalene analogues.

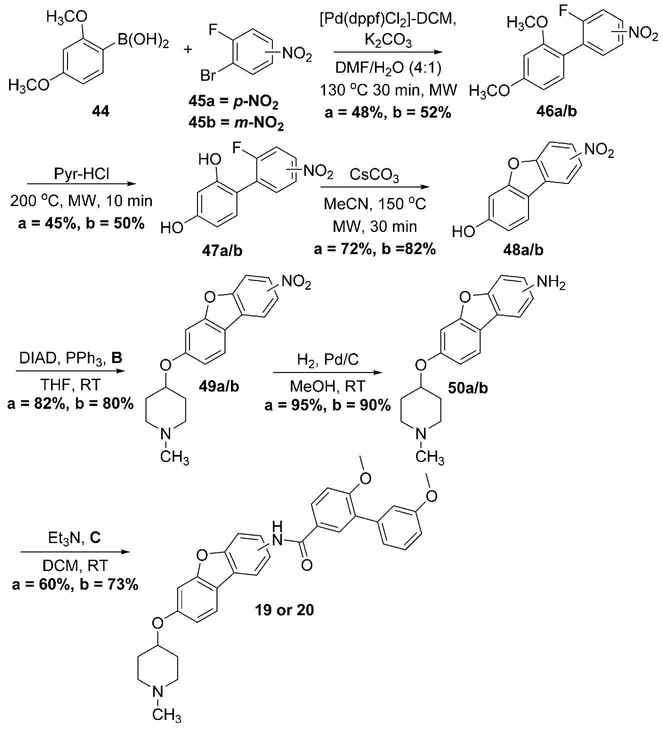

Scheme 4. Synthesis of dibenzo[*b*,*d*]furan analogues.

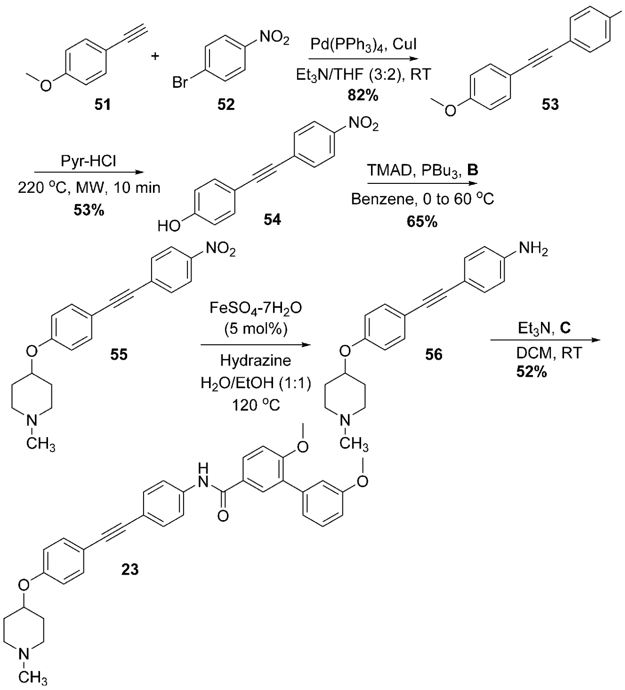

Scheme 5. Synthesis of 1,2-diphenyl-ethyne analogue.

conditions to yield alkyne **53** in 82 % yield. Following cleavage of the methyl ether present in **53**, phenol **54** was treated with *N*-methyl-4-piperidinol under Mitsunobu conditions to furnish **55** in moderate yield. The nitro group on **55** was subsequently reduced,[36] and the resulting aniline was coupled with **C** to produce the final product, **23**.

Evaluation of anti-proliferative activity of analogues

Upon preparation of the compounds listed Table 1, the anti-proliferative activity manifested by these compounds was evaluated against MCF-7 (estrogen receptor positive breast cancer cells), SKBr3 (estrogen receptor negative, HER2 overexpressing breast cancer cells), PC3-MM2 (androgen-independent prostate cancer cells) and MDA-MB-468Ln (human breast cancer triple negative) cell lines (Table 2). In the bicyclic core series, the position of the amide was important for anti-proliferative activity. When the amide was attached at the 1-position, no anti-proliferative activity observed for the aromatic core (in-plane; **7**), whereas moderate activity was observed when the amide was placed out-of-plane (**6**). In contrast, when the amide was placed at the 2-position, an increase in anti-proliferative activity was observed when the amide was in-plane (**57**) versus out-of-plane (**8**).

The anti-proliferative activity manifested by the 2-phenyl-napthalene cores were slightly worse than the 1-phenyl-di(tetra)hydronaphthalene cores and better than the dibenzo[*b*,*d*]-furan cores in the three-ring series. Compounds containing the amide side chain on the phenyl ring (**9**, **11** and **13**) were more active than compounds containing the *N*-methylpiperidine on the phenyl ring (compounds **10**, **12** and **14**), with the *para*-substituted amide analogue being most efficacious for the 2-phenyl-naphthalene series (**13**). When the amide was attached to the *para*-position of the 1-phenyl-di(tetra)hydronaphthalene core, a marginal difference in activity for the di- versus tetrahydronaphthalene core was observed (**17** and **18**). On the other hand, when the amide was placed at the *ortho*-position, an increase in activity against MDA-MB-468Ln and PC3-MM2 cells was observed (**15** and **16**). Finally, there was an increase in activity when the *N*-methylpiperidine was located at the 6-position (**19**) versus the 7-position (**20**) of the dibenzo[*b*,*d*]furan core. The trends observed for these three analogues indicate that compounds are less potent when the rings are fused, versus compounds that can rotate freely.

The incorporation of alkynes into the structure did not produce more potent compounds than their counterparts. For example, **5** exhibits mid-nanomolar activity against all of the cell lines, whereas **23** (which contains an alkyne between the two phenyl rings) manifested a sixfold decrease in activity. A similar trend was also observed between **13** and **29**. Interestingly, when the alkyne of **23** was reduced to the *E*-alkene (**25**), an increase in activity was observed. In contrast, the *Z*-alkene (**24**) exhibited a slight decrease in activity when compared to **23**. However, when **23** was fully saturated, a threefold decrease in activity was observed against the MCF-7 cell line, whereas a twofold increase in activity was observed against SKBr3 cells. These observations highlight the importance of identifying the optimal distance and angle between the *N*-methylpiperidine and the biaryl side chain.

Based on the data outlined in Table 2, three-dimensional graphs[37] were generated to compare the anti-proliferative activity versus the angle and distance between the *N*-methylpiperidine and the biaryl side chain for MCF-7, SKBr3 and PC3-MM2 cell lines (Figure 4). As the angle approaches 180°, the anti-proliferative activity increased in all cell lines. The optimal distance for good anti-proliferative activity (< 2 μM) was variable in these cell lines. In the MCF-7 cell line, the optimal distance for activity was 7.5 to 10.5 Å, although a small pocket was located from 11.5 to 12 Å. In the SKBr3 cell line, the optimal distance was 7.5 to 14 Å. In the PC3-MM2 cell line, the optimal distance for good activity was 7.5 to 10 Å. In general, the most potent compounds (< 1 μM) were those that placed the *N*-methylpiperidine and the biaryl side chain at a 180° angle and between 7.7 to 9.6 Å apart from one another.

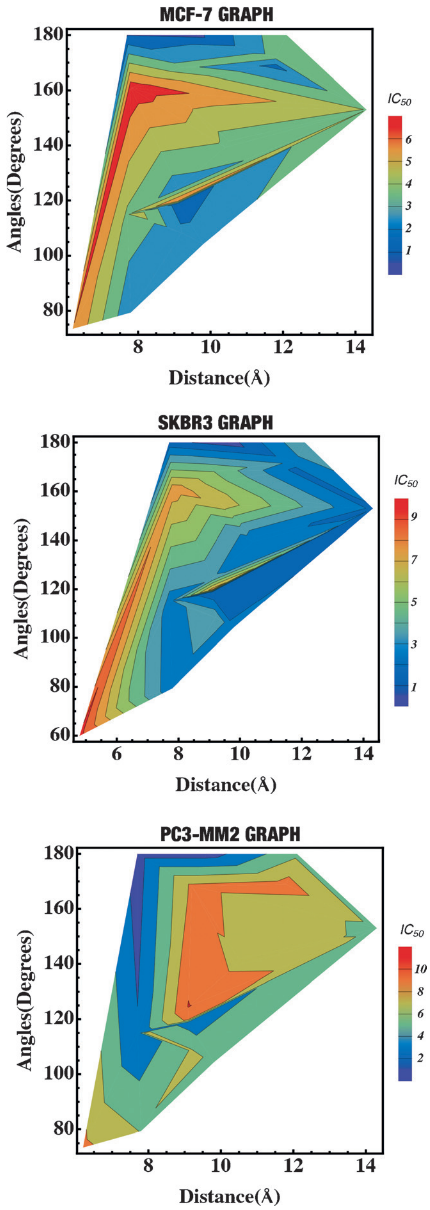

Figure 4. 3D graphs for the anti-proliferative activity versus distance versus angles for MCF-7, SKBr3 and PC3-MM2 cell lines.

Evaluation of Hsp90 inhibitory activity of analogues

After measuring the anti-proliferative activity manifested by these compounds, the molecules were further investigated in the Hsp90-dependent luciferase-refolding assay to correlate Hsp90 inhibitory activity with cell viability.[38] Table 3 lists the compounds that exhibited Hsp90 inhibitory activity. The data in Table 3 was then displayed in a three-dimensional graph, which compares Hsp90 inhibitory activity versus the distance and angle between the *N*-methylpiperidine and the biaryl side chain (Figure 5).

Table 2. Anti-proliferative activity manifested by novobiocin analogues.

Cmpd	Structure	Dist. [Å]	Angle [°]	MCF-7[a]	SKBr3[a]	PC3-MM2[a]	MDA-MB-468Ln[a,d]
6	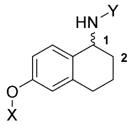	6.2	73.4	5.4 ± 0.80	5.4 ± 0.00	8.7 ± 0.37	7.0
7	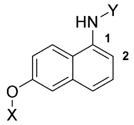	6.3	120	> 50	> 50	> 50	22.1
8	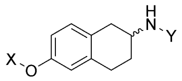	7.8	160.9	6.7 ± 0.00	7.6 ± 0.00	10.7 ± 0.10	12.83
57[b]	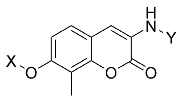	7.8	180	1.5 ± 0.30	1.3 ± 0.22	3.1 ± 0.67	N.T.
9	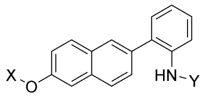	7.7	115	3.9 ± 0.016	2.0 ± 0.016	2.2 ± 0.03	3.0
10	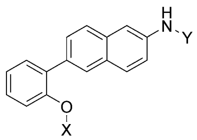	7.9	115	2.6 ± 0.738	3.3 ± 0.05	7.2 ± 1.1	4.3
11	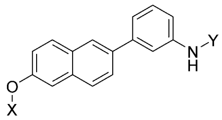	10.4	139.3	2.9 ± 0.639	2.3 ± 0.06	7.5 ± 0.26	3.0
12	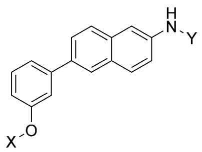	10.5	141.6	2.3 ± 0.13	3.5 ± 0.02	5.7 ± 0.12	3.3
13	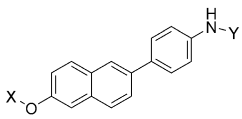	11.8	168.9	1.5 ± 0.139	1.4 ± 0.09	7.9 ± 1.2	2.2
14	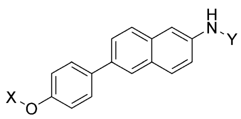	11.8	172.1	3.4 ± 0.09	2.4 ± 0.17	7.49 ± 0.17	4.2
15	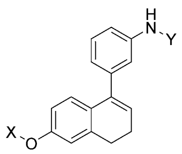	7.8	79.4	2.1 ± 0.03	1.8 ± 0.64	5.2 ± 1.0	3.8
16	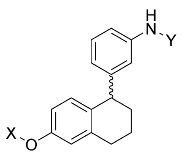	9.1	118.8	1.8 ± 0.43	1.7 ± 0.70	3.3 ± 0.25	2.6

Table 2. (Continued)

Cmpd	Structure	Dist. [Å]	Angle [°]	MCF-7[a]	SKBr3[a]	PC3-MM2[a]	MDA-MB-468Ln[a,d]
17	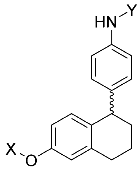	9.2	108.3	2.6 ± 0.63	3.2 ± 0.90	5.4 ± 1.1	1.9
18	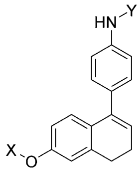	9.8	104.3	2.5 ± 0.40	2.2 ± 0.06	5.6 ± 0.27	3.5
19	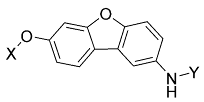	9.1	124.6	2.9 ± 0.58	3.3 ± 0.35	10.3 ± 0.35	5.5
20	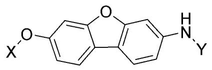	9.4	154.5	4.2 ± 0.80	6.4 ± 0.21	12.0 ± 0.21	> 10
21	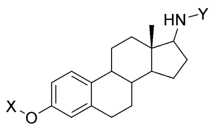	9.2	168.3	3.3 ± 0.37	4.9 ± 0.43	7.9 ± 0.76	5.2
22	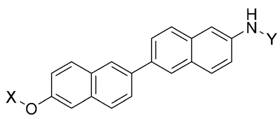	14.1	180	20.9 ± 2.54	11.8 ± 0.94	> 50	> 10
23	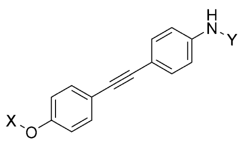	12.1	180	2.7 ± 0.79	4.3 ± 0.01	5.8 ± 0.32	4.9
24	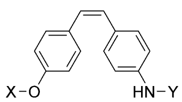	9.1	120	5.9 ± 0.00	7.5 ± 0.00	7.8 ± 1.1	6.0
25	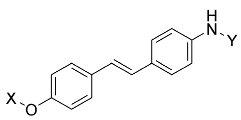	11.8	170.7	1.3 ± 0.59	0.68 ± 0.10	1.3 ± 0.26	0.50
26	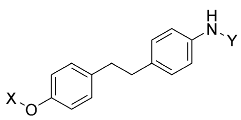	11.9	166.6	9.8 ± 3.4	2.9 ± 1.108	5.3	4.6
5[c]	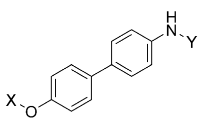	9.6	180	0.71 ± 0.02	0.47 ± 0.06	0.98	N.T.
27	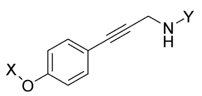	8.7	163	8.7 ± 1.9	14.3 ± 1.20	> 50	26.8
28	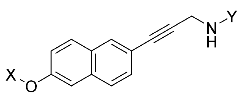	10.9	172.2	8.8	2.2 ± 0.14	2.1 ± 0.41	1.9

Table 2. (Continued)							
Cmpd	Structure	Dist. [Å]	Angle [°]	MCF-7[a]	SKBr3[a]	PC3-MM2[a]	MDA-MB-468Ln[a,d]
29	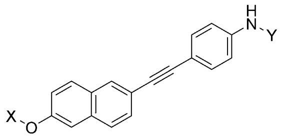	14.3	160.5	4.3±0.42	3.5±0.63	5.4±0.07	2.2

[a] Values are in μM, which represent mean standard deviation for at least two separate experiments performed in triplicate. [b] Reference [31b]. [c] Reference [32a]. N.T. = not tested.

Table 3. Hsp90 inhibitory activity of analogues.

Cmpd	Dist. [Å]	Angle [°]	Hsp90 IC_{50} [μM][a]
6	6.2	73.4	54.7
8	7.8	160.9	118
9	7.7	115	102
14	11.8	172.1	391
57	7.8	180	61.7
15	7.8	79.4	967
16	9.1	118.8	491
18	9.8	104.3	292
19	9.1	124.6	61.2
20	9.4	154.5	149
21	9.2	168.3	115
5	9.6	180	15.8
23	12.1	180	40.9
24	9.1	120	179
25	11.8	170.7	64.9
26	11.9	166.6	85.1
27	8.7	163	266
28	10.9	172.2	821

[a] Values represent mean standard deviation for at least two separate experiments performed in triplicate.

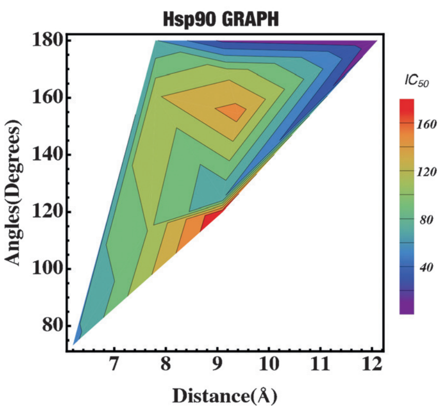

Figure 5. 3D graph for the Hsp90 inhibitory activity versus distance versus angles.

A distance of 6.2 and 12.1 Å between the *N*-methylpiperidine and the biaryl side chain was optimal for Hsp90 inhibitory activity. In general, the distance observed for the compounds in Table 3 fit within the optimal distance identified for the manifestation of good anti-proliferative activity, though there were some exceptions (**6**, **23**). Similar to the anti-proliferation data, the Hsp90 inhibitory activity increased as the angle approached 180°, although exceptions were noted for compounds with a distance of less than 8 Å. There were several compounds that fit within the parameters for distance and angle but did not exhibit Hsp90 inhibitory activity. This information suggests that identification of Hsp90 inhibitors cannot be limited simply to distance and angle. Interestingly, the fused 3- and 4-ring systems (**19**–**21**) were generally more potent Hsp90 inhibitors as compared to the 3-ring systems (**14**, **15**, **16**, **18**) that contained a freely rotatable ring, which was opposite to the observations in the anti-proliferation studies. These data suggest that the Hsp90 inhibitory activity is best for compounds that are flat and exhibit a distance greater than 8 Å.

In order to provide further evidence that the anti-proliferative activity was due to Hsp90 inhibition, Western blot analysis was performed on **25**, which exhibited the most potent anti-proliferative activity and good Hsp90 inhibitory activity. As shown in Figure 6, **25** induced degradation of Hsp90-dependent clients Her2, Raf-1 and CDK6. Actin was used as a control, since this protein is not an Hsp90-dependent substrate.

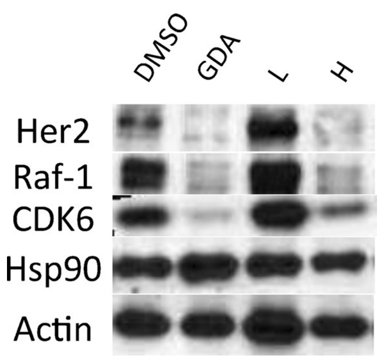

Figure 6. Western blot analyses of Hsp90 client protein degradation in PC3-MM2 cells treated with **25**. L represents a concentration $1/2\times IC_{50}$ value while H represents a concentration of $5\times IC_{50}$ value. Geldanamycin (GDA 500 nM) represents a positive control, while DMSO, represents the negative control.

Conclusions

In this study, the distance and angle between the *N*-methylpiperidine and the biaryl side chain was analyzed in an effort to develop more potent Hsp90 C-terminal inhibitors. The best anti-proliferative and Hsp90 inhibitory activities were obtained when the distance was between 7.7 and 12.1 Å and the angle was close to 180° (Figure 7). As a result of this investigation, a compound (**25**) was developed, which exhibited mid-nanomolar activity against SKBr3 cells. This study also revealed other structural aspects such as planarity and flexibility are important to achieve good anti-proliferative and Hsp90 inhibitory activities. Based on the information gathered in this study, the compounds that exhibited good anti-proliferative and Hsp90 inhibitory activities can be used as a template to develop more novel and useful Hsp90 inhibitors.

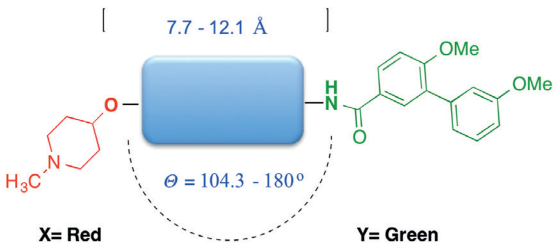

Figure 7. Summary of optimal distance and angle between the *N*-methylpiperidine and the biaryl side chain.

Experimental Section

^{1}H NMR spectra were recorded at 400 or 500 MHz (Bruker DRX-400 Bruker with a H/C/P/F QNP gradient probe) spectrometer and ^{13}C NMR spectra were recorded at 125 MHz (Bruker DRX 500 with broadband, inverse triple resonance, and high resolution magic angle spinning HR-MA probe spectrometer); chemical shifts are reported in δ (ppm) relative to the internal reference [D]$CDCl_3$ ($CDCl_3$, 7.27 ppm). FAB (HRMS) spectra were recorded with a LCT Premier (Waters Corp., Milford, MA) spectrometer. The purity of all compounds was determined to be >95% as determined by ^{1}H NMR and ^{13}C NMR spectroscopy, unless otherwise noted. TLC was performed on glass-backed silica gel plates (Uniplate) with spots visualized by UV light. All solvents were reagent grade and, when necessary, were purified and dried by standard methods. Concentration of solutions after reactions and extractions involved the use of a rotary evaporator operating at reduced pressure.

Acknowledgements

We would like to thank Yusuf Oluwasegun Adeshina and Arnab Bandyopadhyay for producing the 3D graphs for this study. Also, we gratefully acknowledge support of this project by the National Institute of Health (CA120458).

Keywords: antitumor agents · C-terminal inhibitors · Hsp90 · luciferase refolding · medicinal chemistry

[1] J. Trepel, M. Mollapour, G. Giaccone, L. Neckers, *Nat. Rev. Cancer* **2010**, *10*, 537–549.
[2] J. Travers, S. Sharp, P. Workman, *Drug Discovery Today* **2012**, *17*, 242–252.
[3] Y. H. Seo, *Arch. Pharmacal Res.* **2015**, *38*, 1582–1590.
[4] L. Neckers, *J. Biosci.* **2007**, *32*, 517–530.
[5] a) D. Picard, *Cell. Mol. Life Sci.* **2002**, *59*, 1640–1648; b) J. S. Isaacs, W. Xu, L. Neckers, *Cancer Cell* **2003**, *3*, 213–217; c) W. B. Pratt, D. O. Toft, *Exp. Biol. Med.* **2003**, *228*, 111–133; d) L. Whitesell, S. L. Lindquist, *Nat. Rev. Cancer* **2005**, *5*, 761–772.
[6] C. Moser, S. A. Lang, O. Stoeltzing, *Anticancer Res.* **2009**, *29*, 2031–2042.
[7] F. Koga, K. Kihara, L. Neckers, *Anticancer Res.* **2009**, *29*, 797–807.
[8] J. Franke, S. Eichner, C. Zeilinger, A. Kirschning, *Nat. Prod. Rep.* **2013**, *30*, 1299–1323.
[9] A. Khandelwal, V. Crowley, B. S. J. Blagg, *Med. Res. Rev.* **2015**, *35*, 92–118.
[10] K. Jhaveri, S. Modi, *Onco Targets Ther.* **2015**, *8*, 1849–1858.
[11] D. S. Hong, U. Banerji, B. Tavana, G. C. George, J. Aaron, R. Kurzock, *Cancer Treat. Rev.* **2013**, *39*, 375–387.
[12] a) S. N. Shelton, M. E. Shawgo, S. B. Matthews, Y. Lu, A. C. Donnelly, K. Szabla, M. Tanol, G. A. Vielhauer, R. A. Rajewski, R. L. Matts, B. S. Blagg, J. D. Robertson, *Mol. Pharmacol.* **2009**, *76*, 1314–1322; b) R. Conde, Z. R. Belak, M. Nair, R. F. O'Carroll, N. Ovsenek, *Biochem. Cell Biol.* **2009**, *87*, 845–851.
[13] A. Donnelly, B. S. J. Blagg, *Curr. Med. Chem.* **2008**, *15*, 2702–2717.
[14] I. Gomez-Monterrey, M. Sala, S. Musella, P. Campiglia, *Recent Pat. Anti-Cancer Drug Discov.* **2012**, *7*, 313–336.
[15] X. Song, Z. Zhao, X. Qi, S. Tang, Q. Wang, T. Zhu, Q. Gu, M. Liu, J. Li, *Oncotarget.* **2015**, *6*, 5263–5274.
[16] Y. Wang, S. R. McAlpine, *Org. Biomol. Chem.* **2015**, *13*, 4627–4631.
[17] M. Strocchia, S. Terracciano, M. G. Chini, A. Vassallo, M. C. Vaccaro, F. Dal Piaz, A. Leone, R. Riccio, I. Bruno, G. Bifulco, *Chem. Commun.* **2015**, *51*, 3850–3853.
[18] Y. Wang, S. R. McAlpine, *Chem. Commun.* **2015**, *51*, 1410–1413.
[19] J. Gavenonis, N. E. Jonas, J. A. Kritzer, *Bioorg. Med. Chem.* **2014**, *22*, 3989–3993.
[20] J. Davenport, J. R. Manjarrez, L. Peterson, B. Krumm, B. S. J. Blagg, R. L. Matts, *J. Nat. Prod.* **2011**, *74*, 1085–1092.
[21] A. Khandelwal, J. A. Hall, B. S. J. Blagg, *J. Org. Chem.* **2013**, *78*, 7859–7884.
[22] Z. Yin, E. C. Henry, T. A. Gasiewicz, *Biochemistry* **2009**, *48*, 336–345.
[23] M. K. Hadden, L. Galam, J. E. Gestwicki, R. L. Matts, B. S. J. Blagg, *J. Nat. Prod.* **2007**, *70*, 2014–2018.
[24] H. Zhao, G. E. Brandt, L. Galam, R. L. Matts, B. S. J. Blagg, *Bioorg. Med. Chem. Lett.* **2011**, *21*, 2659–2664.
[25] M. G. Marcu, A. Chadli, I. Bouhouche, M. Catelli, L. M. Neckers, *J. Biol. Chem.* **2000**, *275*, 3718137186.
[26] M. G. Marcu, T. W. Schulte, L. Neckers, *J. Natl. Cancer Inst.* **2000**, *92*, 242–248.
[27] R. L. Matts, A. Dixit, L. B. Peterson, L. Sun, S. Voruganti, P. Kalyanaraman, S. D. Hartson, G. M. Verkhivker, B. S. J. Blagg, *ACS Chem. Biol.* **2011**, *6*, 800–807.
[28] E. Moroni, H. Zhao, B. S. J. Blagg, G. Colombo, *J. Chem. Inf. Model.* **2014**, *54*, 195–208.
[29] S. Sattin, J. Tao, G. Vettoretti, E. Moroni, M. Pennati, A. Lopergolo, L. Morelli, A. Bugatti, A. Zuehlke, M. Moses, T. Prince, T. Kijima, K. Beebe, M. Rusnati, L. Neckers, N. Zaffaroni, D. A. Agard, A. Bernardi, G. Colombo, *Chem. Eur. J.* **2015**, *21*, 13598–15608.
[30] a) G. Garg, H. Zhao, B. S. J. Blagg, *ACS Med. Chem. Lett.* **2015**, *6*, 204–209; b) J. A. Hall, L. K. Forsberg, B. S. J. Blagg, *Future Med. Chem.* **2014**, *6*, 1587–1605; c) J. Zhao, H. Zhao, J. A. Hall, D. Brown, E. Brandes, J. Bazzill, P. T. Grogan, C. Subramanian, G. Vielhauer, M. S. Cohen, B. S. J. Blagg, *MedChemComm* **2014**, *5*, 1317–1323; d) H. Zhao, E. Moroni, G. Colombo, B. S. J. Blagg, *ACS Med. Chem. Lett.* **2014**, *5*, 84–88; e) H. Zhao, B. Yan, L. B. Peterson, B. S. J. Blagg, *ACS Med. Chem. Lett.* **2012**, *3*, 327–331; f) B. R. Kusuma, L. B. Peterson, H. Zhao, G. Vielhauer, J. Holzbeierlein, B. S. J. Blagg, *J. Med. Chem.* **2011**, *54*, 6234–6253; g) J. A. Burlison, L. Neckers, A. B. Smith, A. Maxwell, B. S. J. Blagg, *J. Am. Chem. Soc.* **2006**, *128*, 15529–15536; h) J. A. Burlison, B. S. J. Blagg, *Org. Lett.* **2006**, *8*, 4855–4858; i) X. M. Yu, G. Shen, L. Neckers, H. Blake, J. Holzbeierlein, B. Cronk, B. S. J. Blagg, *J. Am. Chem. Soc.* **2005**, *127*, 12778–12779.
[31] a) H. Zhao, B. R. Kusuma, B. S. J. Blagg, *ACS Med. Chem. Lett.* **2010**, *1*, 311–315; b) H. Zhao, A. C. Donnelly, B. R. Kusuma, G. E. L. Brandt, D. Brown, R. A. Rajewski, G. Vielhauer, J. Holzbeierlein, M. S. Cohen, B. S. J. Blagg, *J. Med. Chem.* **2011**, *54*, 3839–3853.
[32] a) H. Zhao, G. Garg, J. Zhao, E. Moroni, A. Girgis, L. S. Franco, S. Singh, G. Colombo, B. S. J. Blagg, *Eur. J. Med. Chem.* **2015**, *89*, 442–466; b) H.

Zhao, M. Anyika, A. Girgis, B. S. J. Blagg, *Bioorg. Med. Chem. Lett.* **2014**, *24*, 3633 – 3637.
[33] T. Tsunoda, Y. Yamamiya, Y. Kawamura, S. Itô, *Tetrahedron Lett.* **1995**, *36*, 2529 – 2530.
[34] E. Richmond, N. Duguet, A. M. Z. Slawin, T. Lébl, A. D. Smith, *Org. Lett.* **2012**, *14*, 2762 – 2765.
[35] T. H. Jepsen, M. Larsen, M. Jørgensen, M. B. Nielsen, *Synthesis* **2013**, *45*, 1115 – 1120.
[36] U. Sharma, P. K. Verma, N. Kumar, V. Kumar, M. Bala, B. Singh, *Chem. Eur. J.* **2011**, *17*, 5903 – 5907.
[37] Wolfram Research, Inc., Mathematica, Version 10.3, Champaign, IL 2015.
[38] a) L. Galam, K. M. Hadden, Z. Ma, Q. Z. Ye, B. G. Yun, B. S. J. Blagg, R. L. Matts, *Bioorg. Med. Chem.* **2007**, *15*, 1939 – 1946; b) T. Sadikot, M. Swink, J. D. Eskew, D. Brown, H. Zhao, B. R. Kusuma, R. A. Rajewski, B. S. J. Blagg, R. L. Matts, J. M. Holzbeirlein, G. A. Vielhauer, *Assay Drug Dev. Technol.* **2013**, *11*, 478 – 488.

Received: December 9, 2015
Revised: February 11, 2016
Published online on April 1, 2016